Title
Atomic Resolution Imaging of Halide Perovskites.

Journal
Nano letters, 16(12)

ISSN
1530-6984

Authors
Yu, Yi
Zhang, Dandan
Kisielowski, Christian
et al.

Publication Date
2016-12-01

DOI
10.1021/acs.nanolett.6b03331

Peer reviewed

NANO LETTERS

Letter

pubs.acs.org/NanoLett

Atomic Resolution Imaging of Halide Perovskites

Yi Yu,[†,‡] Dandan Zhang,[†,‡] Christian Kisielowski,[§] Letian Dou,[†,‡] Nikolay Kornienko,[†,‡] Yehonadav Bekenstein,[†,‡] Andrew B. Wong,[†,‡] A. Paul Alivisatos,[†,‡,∥,⊥] and Peidong Yang*[,†,‡,∥,⊥]

[†]Department of Chemistry, University of California, Berkeley, California 94720, United States

[‡]Materials Sciences Division and [§]The Molecular FoundryLawrence Berkeley National Laboratory, Berkeley, California 94720, United States

[∥]Kavli Energy NanoScience Institute, Berkeley, California 94720, United States

[⊥]Department of Materials Science and Engineering, University of California, Berkeley, California 94720, United States

Supporting Information

ABSTRACT: The radiation-sensitive nature of halide perovskites has hindered structural studies at the atomic scale. We overcome this obstacle by applying low dose-rate in-line holography, which combines aberration-corrected high-resolution transmission electron microscopy with exit-wave reconstruction. This technique successfully yields the genuine atomic structure of ultrathin two-dimensional $CsPbBr_3$ halide perovskites, and a quantitative structure determination was achieved atom column by atom column using the phase information on the reconstructed exit-wave function without causing electron beam-induced sample alterations. An extraordinarily high image quality enables an unambiguous structural analysis of coexisting high-temperature and low-temperature phases of $CsPbBr_3$ in single particles. On a broader level, our approach offers unprecedented opportunities to better understand halide perovskites at the atomic level as well as other radiation-sensitive materials.

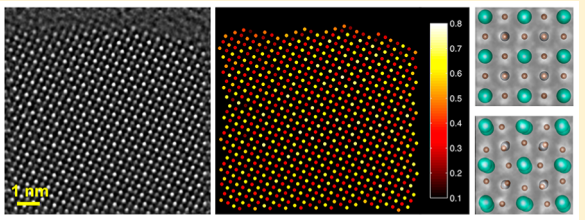

KEYWORDS: *Atomic resolution, halide perovskites, low dose-rate, in-line holography, radiation-sensitive materials*

Halide perovskites have great potential for many applications such as high-efficiency photovoltaic cells.[1] Research addressing these materials, in particular their nanostructures, has recently attracted worldwide attention. Various morphologies of halide perovskites, such as quantum dots,[2,3] nanowires,[4] nanosheets (NSs),[4−6] and thin films,[1] have been fabricated and their optoelectronic properties were explored. However, structure−property relationships are difficult to extract because atomic resolution imaging of halide perovskites by transmission electron microscopy (TEM) is greatly impeded by destructive electron beam-sample interactions.[4−7]

Conventional TEM, aberration-corrected TEM (AC-TEM), and aberration-corrected scanning transmission electron microscopy (AC-STEM) have greatly contributed to the characterization of oxide perovskites with a spatial resolution less than one angstrom.[8,9] As a result of such investigations, the correlation of structure with chemical and physical properties contributes to the discovery and understanding of novel and unique properties in these materials.[10−12] By comparison, a precise understanding of halide perovskites is relatively underdeveloped because of their electron beam-sensitivity[4−7] that prohibits capturing high-resolution TEM (HRTEM) or AC-HRTEM images with commonly used electron dose rates of 10^4−10^5 e $Å^{-2}$ s^{-1}. The acquisition of HRSTEM or AC-HRSTEM images in no way relaxes this situation as these methods require even larger electron doses to form images.[13,14] Making things even more challenging, electron-beam induced sample alterations occur much more quickly and severely in nanosized halide perovskites compared to the bulk material. Therefore, structural characterizations using electron beams generally have to be performed at low magnifications, where the required dose-rate to obtain sufficient contrast is much lower. Even in this situation, structural damage occurs and is evident as tiny precipitates or voids in reported TEM and STEM images.[4−7] Therefore, a very limited number of conventional HRTEM images supported reports[2−6] and the images suffered from varying degrees of blurring or distortion caused by the imaging electrons. Clearly, it is hardly possible to make further progress without addressing the problem of sample degradation during observation. So far, faithful atomic resolution images have been neither captured by electron microscopy nor any other experimental techniques for these materials.

In the present work, we visualize for the first time the pristine structure of ultrathin two-dimensional (2D) $CsPbBr_3$ halide perovskites with atomic resolution by applying low dose-rate in-line holography. This emerging method minimizes electron beam-induced sample alterations by effectively controlling electron beam-induced object excitations.[15] This is a low dose

Received: August 8, 2016
Revised: October 17, 2016

DOI: 10.1021/acs.nanolett.6b03331
Nano Lett. XXXX, XXX, XXX−XXX

technique that retards structural damage while high signal-to-noise are generated by recording an image series that is subsequently reconstructed to extract the phase information and recover electron exit-wave functions[16−18] (In general, phase information is always missing in TEM images where only amplitude information preserves.) This process provides valuable phase information that enables a quantitative structure determination of 2D NSs on the basis of detecting the element-specific contrast from single atoms.

Atomically thin 2D $CsPbBr_3$ NSs were successfully synthesized via a catalyst-free, solution-phase method (SI section 1). The NSs were characterized using X-ray diffraction (XRD) (Figure S1a), low-magnification TEM and STEM (Figure S1b), energy-dispersive X-ray spectroscopy (EDS) (Figure S2a), and atomic force microscopy (AFM) (Figure S2b). The edge length of $CsPbBr_3$ NSs was measured to be around 100 nm, while the thickness of the NSs was a few atomic layers. An AFM image of NSs with 1−3 layer thickness is depicted in Figure S2b. The $CsPbBr_3$ bulk crystals exhibit a cubic structure at high temperature (above 403 K) and an orthorhombic crystal structure at room temperature. The cubic unit cell of $CsPbBr_3$ is illustrated in Figure 1a and a model of a 2D monolayer is depicted in Figure 1b. The difference between the cubic and orthorhombic structures lies in the tilting of the $Pb-Br_6$ octahedrons in the orthorhombic case, which is difficult to capture with standard TEM techniques. Previous reports suggest that the high-temperature phase could be stabilized in quantum dots and NSs.[2,5,6] However, we emphasize that Scherrer peak broadening in nanocrystals sometimes impedes the ability to distinguish the orthorhombic phase from the cubic one by peak-splitting (Figure S1a). Therefore, assignment of phases simply by conventional XRD as previously reported is insufficient and direct atomic resolution imaging is mandatory for unambiguous structure determination.

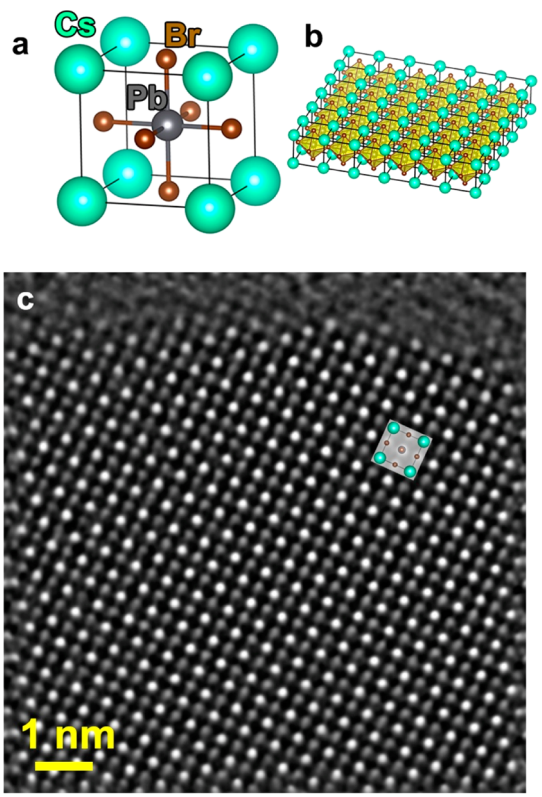

Figure 1. Atomic resolution image of 2D halide perovskite $CsPbBr_3$. (a) Structure model of cubic $CsPbBr_3$ perovskite unit cell. Cs (green) occupies the corner A-site while Pb (gray) occupies the body-center B-site, and Br (brown) occupies the face-center. $Pb-Br_6$ octahedron is formed within the Cs cube framework. (b) Structure model of single layer 2D $CsPbBr_3$ NS. (c) Atomically resolved phase image of a 2D $CsPbBr_3$ NS obtained by reconstructing 80 low dose-rate AC-HRTEM images via exit-wave reconstruction. The [001] structure projection of a unit cell is overlaid on the image.

The ultrathin nature of $CsPbBr_3$ 2D NSs renders them prone to electron beam-induced alterations (Figures S3 and S4). We have performed comparative experiments at different accelerating voltages (80 kV and 300 kV) using different imaging modes (TEM and STEM) to explore how to minimize electron beam-induced sample alterations and achieve atomic resolution. In particular, we use low dose AC-HRTEM at 80 kV (SI Sections 7 and 8) to capture in-line holograms. The method addresses the shot noise problem in low dose images by acquiring an image series and solving the phase problem to reconstruct exit-wave functions.[16−18] For a typical reconstruction process, a focal-series of 10−100 images is recorded to recover the specimen's exit-wave function, which contains the full information from the elastic scattering process in the form of amplitude and phase images over the spatial frequencies that are relevant to form atomically resolved images. All of this data is intrinsically quantitative and can be fine-tuned even further by a posteriori aberration correction using numerical wave processing.[19−21] The reconstructed wave function from low dose-rate images represents a time average over the duration of the recording time that exhibits a better signal-to-noise ratio because it eliminates the well-known contrast reduction by the Stobbs factor and constitutes a weak-excitation approach that improves on sample integrity.[15] Therefore, the pristine structure of nanocrystals can be better maintained by this low dose-rate technique.

An example of a focal-series containing 80 AC-HRTEM images that were acquired at the edge of a $CsPbBr_3$ NS with a dose-rate of ~100 e $Å^{-2}$ s^{-1} is shown in Figure S5a. The exit-wave was reconstructed from all the 80 images and the reconstructed phase image is shown in Figure 1c. It is evident that all the atom columns are clearly resolved and the contrast is homogeneous across the whole image. The homogeneous contrast is only possible if formation of vacancies, voids, or other electron beam-induced precipitates does not occur. The same conclusion can be derived by directly inspecting the contrast of all 80 sequential images (Figure S5a). The $CsPbBr_3$ NS in Figure 1c shows a perfect cubic perovskite structure in the [001] projection with the Cs atom columns and Pb−Br atom columns exhibiting higher contrast while the Br atom columns show weaker contrast. The cubic [001] atomic model is overlaid on Figure 1c and matches the experimental atom positions. The distinction between Cs columns and Pb−Br columns can be achieved by a quantitative statistical phase analysis as detailed later. The contrast maxima in Figure 1c mark the atom column positions while the intensities correspond to phase values that are determined by their chemical composition. Therefore, all necessary information can be extracted to characterize the crystal structure. The result is shown in Figure 2a. Atom positions were obtained by a least-squares fit to the intensity distribution around contrast maxima using 2D Gaussian profiles.[22] Phase changes were characterized by the peak-to-valley intensities of each atom column. Element specific phase changes are larger for Cs and Pb−Br columns

DOI: 10.1021/acs.nanolett.6b03331
Nano Lett. XXXX, XXX, XXX−XXX

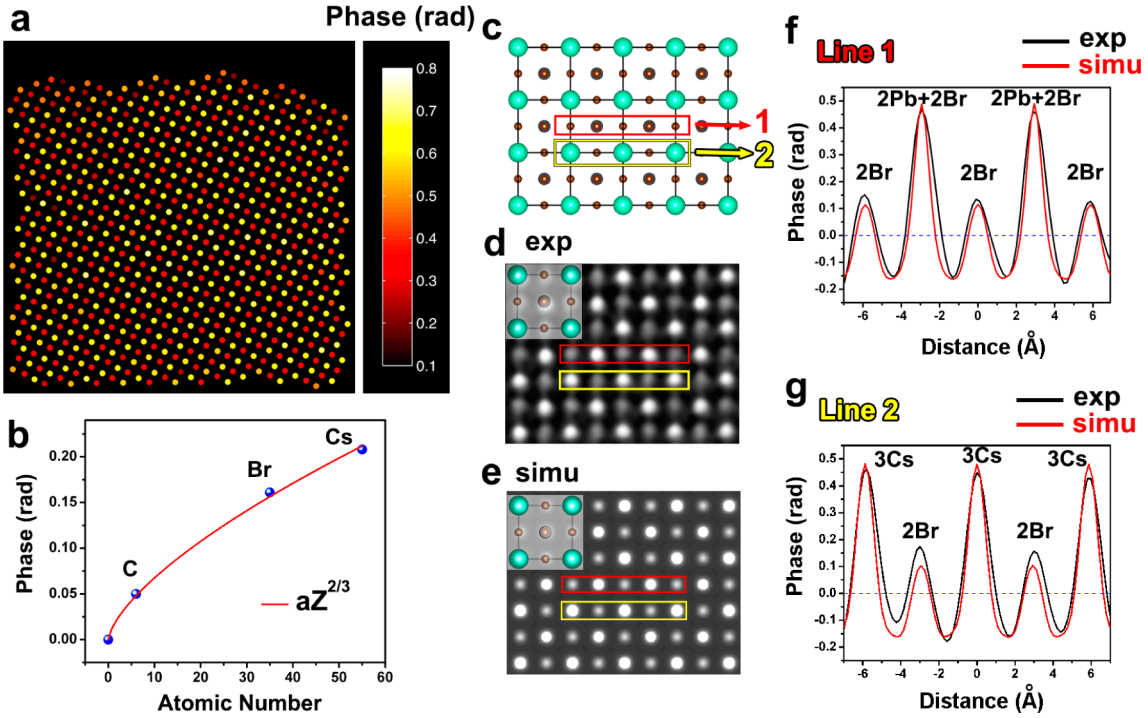

Figure 2. Quantitative phase analysis. (a) Atomic-scale 2D phase mapping. (b) Plot of the single atom-induced phase changes of different atom species versus their atomic number, Z. The red curve shows the fitting to the power law $aZ^{2/3}$, where a is a constant. Br and Cs data come from this work, while the data for C come from refs 23 and 24. (c) Model of [001] structural projection (4 unit cell by 3 unit cell). (d) Enlarged experimental phase image from a region in the center of Figure 1c. The structural model is overlaid. (e) Simulated phase image corresponds to (d). (f,g) Line profiles of two line scans (f shows line 1 and g shows line 2) as indicated in (c–e). In the profiles, black lines correspond to the experiments and red lines correspond to the simulations.

(yellow color) but smaller for Br columns (red color) because it is a lighter element. The small scattering difference between Cs columns and Pb–Br columns can only be distinguished by comparing the average phase values of the different lattice sites because the heavier Pb–Br columns should have slightly larger phase change because of the electron channeling effect.[20] A statistical analysis reveals that average phase values of the Cs, Pb–Br, and Br atom columns are 0.625 ± 0.006, 0.640 ± 0.006, and 0.322 ± 0.004 rad, respectively, with a 95% confidence level. These small error bars are the key to differentiate between Cs and Pb–Br columns experimentally and are in agreement with our simulation (Figure S7).

Within an extinction distance for electron channeling, the phase increases linearly with depth.[20] Hence, it is not only possible to determine the crystal structure and to identify elements but also to determine the crystal thickness. Figure 2d shows an enlarged phase image extracted from the center of Figure 1c. The corresponding structural projection is depicted in Figure 2c. For comparison, a simulated phase image of a two-atomic-layer-thick $CsPbBr_3$ NS is shown in Figure 2e. Two line profiles are extracted from the experimental and simulated phase images, and the results are shown in Figure 2f,g, respectively. The quantitative match between experimental and simulated data indicates that the $CsPbBr_3$ NS of Figure 1c is composed of only two atomic layers (also see Figure S8). Knowing the crystal thickness in terms of the number of atoms per column, we can further obtain the characteristic phase shift per single atom. The scattering of 80 kV electrons at single Cs and Br atoms were calculated 0.208 ± 0.002 and 0.161 ± 0.002 rad, respectively, and these are depicted in Figure 2b together with an experimental value for the phase shift at a single carbon atom reported previously.[23,24] All the data can be described well by the power law for phase shifts caused by electron scattering from a single atom that is expected to be roughly proportional to $Z^{2/3}$ (Z is the atomic number).[25,26] Independently of our image simulation, these quantitative phase measurements can be used to support the interpretation that our $CsPbBr_3$ NS are indeed double-layers. Moreover, we can also compare individual AC-HRTEM images of the focal-series with corresponding simulated images at the measured focus values. We found that experimental images fit well with the simulation when the thickness is assumed to be a double-layer (Figures S5b and Figure S6). Therefore, low dose-rate in-line holography not only reveals the pristine structure of beam-sensitive materials with atomic resolution but also allows identifying elements together with the local column thickness, which enables electron tomography from single projections.

Beyond a description of crystallographically perfect $CsPbBr_3$ NSs, it is interesting to study structural deviations. Apart from cubic structure, we have also observed orthorhombic domains in some of the 2D NSs. Awareness of a possible coexistence of both the high-temperature cubic phase and the room-temperature orthorhombic phase is of value to the community. Different from the ensemble-level information obtained from X-ray techniques, our atomic-scale direct imaging method on the singe sheet level enables us to explore the structure more deeply. The existence of the orthorhombic structure as well as the coexistence of two phases can be confirmed using in-line holography with different dose-rates. The results are depicted in Figures S9 and S10. More details of coexistence of two phases are provided in the SI Section 11. Here, apart from using the in-line holography method, we demonstrate that a single AC-

DOI: 10.1021/acs.nanolett.6b03331
Nano Lett. XXXX, XXX, XXX–XXX

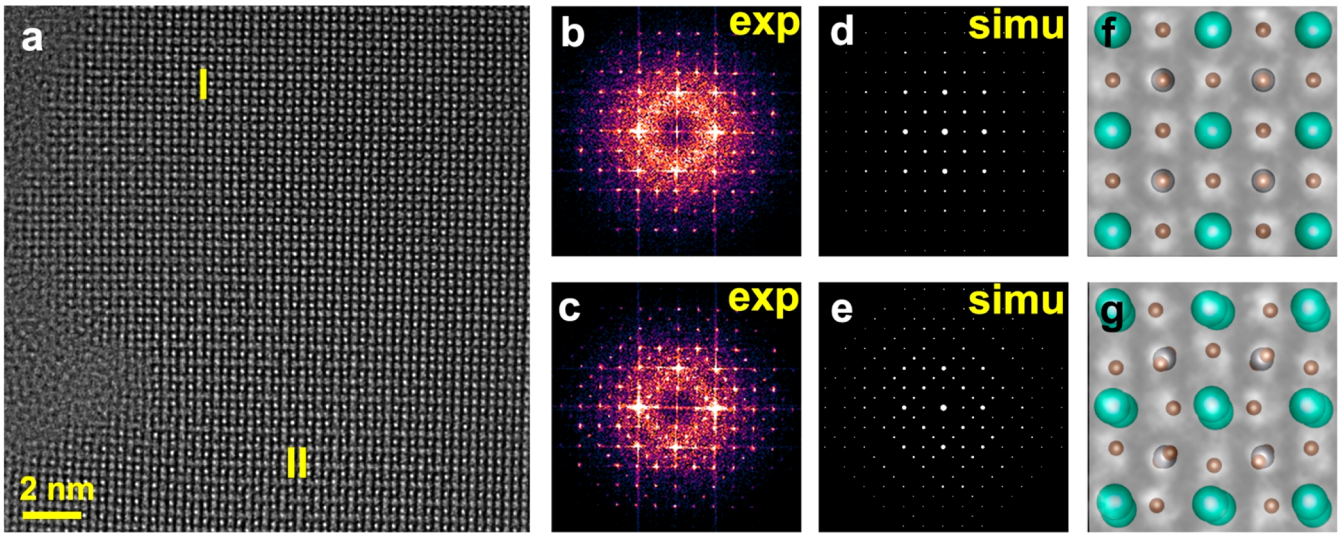

Figure 3. Coexistence of cubic and orthorhombic $CsPbBr_3$ within single AC-HRTEM image. (a) Experimental AC-HRTEM image with two regions denoted as I and II. (b,c) Experimental Fourier transforms from region I (b) and II (c). (d,e) Simulated electron diffraction of cubic (d) and orthorhombic (e) $CsPbBr_3$. (f,g) Enlarged images from region I (f) and II (g). The cubic and orthorhombic structure models are overlaid on (f) and (g), respectively.

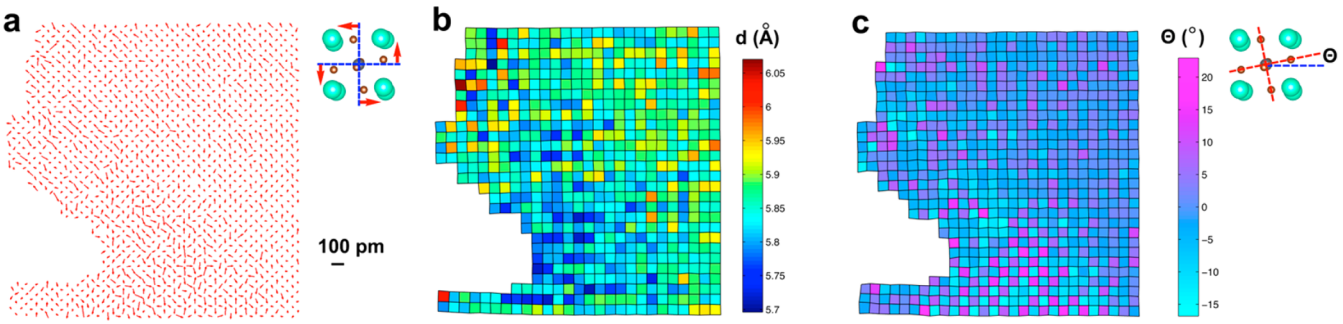

Figure 4. Quantitative structure analysis. (a) Br displacement map. The Br displacement is defined as the deviation of Br columns from the center of two neighboring Cs columns, as illustrated in the upper right model. The length of the red arrows represents the modulus of the displacements with respect to the scale bar in the lower right corner. The arrowheads point into the displacement directions. (b) Lattice distance map. The lattice distance is defined as the distance between two neighboring Pb−Br columns. (c) Octahedron tilting map. The tilting angle is defined as the model shown on the upper right corner.

HRTEM image can also be utilized to determine structural details as long as the dose-rate is sufficiently controlled and the material can maintain its structure at the given dose-rate. Figure 3a is an AC-HRTEM image from the edge of a $CsPbBr_3$ NS recorded with the dose-rate of 3800 e $Å^{-2}$ s^{-1} (exposure time 1 s). By imaging with an optimum focus and a negative spherical-aberration,[8,22] we also obtain a direct structure image with Cs and Pb−Br columns exhibiting a brighter contrast compared to the Br columns. Looking into the details of the atomic structure, we notice that the lower region (marked as II) of Figure 3a differs structurally compared to the upper region (marked as I). The difference is most evident in the corresponding Fourier transforms of regions I and II as shown in Figure 3b,c, respectively. The simulations of the electron diffraction patterns of cubic and orthorhombic $CsPbBr_3$ in a [001] zone axis orientation are provided in Figure 3d,e, respectively. Comparing the experimental data with the simulation, we can conclude that we observe the case of a mixed structure where region I crystallized in the cubic structure while region II is in the orthorhombic structure. Figure 3f,g shows enlarged images from region I and II, respectively, with the atomic structural model overlaid. Experimental images agree well with the structure models, and the tilting of the Pb−Br_6 octahedrons in the orthorhombic phase is directly observable.

A further quantitative examination allows us to extract additional complementary information. First, the Br displacement map shown in Figure 4a reveals that the lower region exhibits larger displacements from the midpoint between two neighboring Cs columns as a result of tilting octahedrons in orthorhombic structure. This clearly marks the boundary between the orthorhombic and cubic phases. Second, we have measured lattice parameters unit cell by unit cell and the result is shown in Figure 4b. For bulk $CsPbBr_3$, the distance between Pb−Br columns in [001] projection differs by only 5 pm between cubic (5.87 Å) and orthorhombic structure (5.82 Å). Experimentally for the 2D NS, both the cubic and orthorhombic phases exhibit a lattice expansion compared to their bulk counterpart, but this map can still identify the orthorhombic region from the map as it exhibits smaller distances (blue color). The presence of a lattice expansion in ultrathin 2D $CsPbBr_3$ NSs is confirmed by our grazing-incidence wide-angle X-ray scattering (GIWAXS) experiments (Figure S13). Finally, we have measured the tilting angle of the

DOI: 10.1021/acs.nanolett.6b03331
Nano Lett. XXXX, XXX, XXX−XXX

Pb−Br_6 octahedrons and the tilting map is shown in Figure 4c. The chessboard pattern in the lower region is another clear confirmation that the orthorhombic structure is present. These results may have relevance for the understanding of the growth and structure−property relationship in the halide perovskite materials.

The combination of dose controlled AC-HRTEM imaging and low dose-rate in-line holography enables atomic resolution imaging of halide perovskites without introducing structural damages in $CsPbBr_3$. The crystallographic structure of plate shaped nanocrystals is revealed at atomic resolution with single atom sensitivity. A reproducible determination of absolute phase values for electrons that are scattering at single atoms shows that the method has become fully quantitative if beam-sample interactions are controlled. We fully characterize coexisting high-temperature and low-temperature phases that are studied in this manner. Importantly, the method can be applied to any beam-sensitive material and does not require uncommon TEM attachments so that it can be easily popularized in most of the laboratories. This work shows that another door opened for atomic resolution imaging of beam-sensitive materials in general, and it can be further explored and developed, such as utilizing direct electron detection[27] or complementing with other low dose techniques.[28,29]

■ ASSOCIATED CONTENT

Supporting Information

The Supporting Information is available free of charge on the ACS Publications website at DOI: 10.1021/acs.nanolett.6b03331.

Details of materials synthesis, characterization methods, image processing and simulations, and first-principle calculations. Discussions of electron beam-sample interaction, low dose-rate imaging, and coexistence of cubic and orthorhombic phases (PDF)

■ AUTHOR INFORMATION

Corresponding Author

*E-mail: p_yang@berkeley.edu.

Author Contributions

Y.Y. and P.Y. designed the experiments. Y.Y. performed TEM experiments, simulations, and data analysis. D.Z. carried out the synthesis of halide perovskite samples and performed XRD experiments. C.K. contributed to the data analysis. L.D. performed AFM experiments. N.K. performed GIWAXS experiments. Y.B. and A.B.W. contributed to the data analysis and manuscript preparation. Y.Y., C.K., and P.Y. wrote the manuscript. C.K. supervised the low dose-rate experiments. A.P.A. and P.Y. supervised the research project. All authors contributed to the discussions.

Notes

The authors declare no competing financial interest.

■ ACKNOWLEDGMENTS

This work was supported by the Physical Chemistry of Inorganic Nanostructures Program, KC3103, Office of Basic Energy Sciences of the United States Department of Energy under Contract No. DE-AC02-05CH11231. TEM Work at the NCEM, Molecular Foundry, and GIWAXS measurements at beamline 7.3.3 at the Advanced Light Source (ALS), were supported by the Office of Science, Office of Basic Energy Science, of the U.S. Department of Energy under Contract No. DE-AC02-05CH11231. We would like to thank Chenhui Zhu for help with GIWAXS measurements.

■ REFERENCES

(1) Liu, M.; Johnston, M. B.; Snaith, H. J. Efficient planar heterojunction perovskite solar cells by vapour deposition. *Nature* **2013**, *501*, 395−398.

(2) Protesescu, L.; Yakunin, S.; Bodnarchuk, M. I.; Krieg, F.; Caputo, R.; Hendon, C. H.; Yang, R. X.; Walsh, A.; Kovalenko, M. V. Nanocrystals of Cesium Lead halide perovskites ($CsPbX_3$, X = Cl, Br, and I): Novel optoelectronic materials showing bright emission with wide color gamut. *Nano Lett.* **2015**, *15*, 3692−3696.

(3) Cottingham, P.; Brutchey, R. L. On the crystal structure of colloidally prepared $CsPbBr_3$ quantum dots. *Chem. Commun.* **2016**, *52*, 5246−5249.

(4) Zhang, D.; Eaton, S. W.; Yu, Y.; Dou, L.; Yang, P. Solution-phase synthesis of Cesium Lead halide perovskite nanowires. *J. Am. Chem. Soc.* **2015**, *137*, 9230−9233.

(5) Bekenstein, Y.; Koscher, B. A.; Eaton, S. W.; Yang, P.; Alivisatos, A. P. Highly luminescent colloidal nanoplates of perovskite Cesium Lead halide and their oriented assemblies. *J. Am. Chem. Soc.* **2015**, *137*, 16008−16011.

(6) Akkerman, Q. A.; Motti, S. G.; Kandada, A. R. S.; Mosconi, E.; D'Innocenzo, V.; Bertoni, G.; Marras, S.; Kamino, B. A.; Miranda, L.; De Angelis, F.; Petrozza, A.; Prato, M.; Manna, L. Solution synthesis approach to colloidal Cesium Lead halide perovskite nanoplatelets with monolayer-level thickness control. *J. Am. Chem. Soc.* **2016**, *138*, 1010−1016.

(7) Dou, L.; Wong, A. B.; Yu, Y.; Lai, M.; Kornienko, N.; Eaton, S. W.; Fu, A.; Bischak, C. G.; Ma, J.; Ding, T.; Ginsberg, N. S.; Wang, L. W.; Alivisatos, A. P.; Yang, P. Atomically thin two-dimensional organic-inorganic hybrid perovskites. *Science* **2015**, *349*, 1518−1521.

(8) Jia, C. L.; Lentzen, M.; Urban, K. Atomic-resolution imaging of oxygen in perovskite ceramics. *Science* **2003**, *299*, 870−873.

(9) Muller, D. A.; Kourkoutis, L. F.; Murfitt, M.; Song, J. H.; Hwang, H. Y.; Silcox, J.; Dellby, N.; Krivanek, O. L. Atomic-scale chemical imaging of composition and bonding by aberration-corrected microscopy. *Science* **2008**, *319*, 1073−1076.

(10) Jia, C. L.; Mi, S. B.; Urban, K.; Vrejoiu, I.; Alexe, M.; Hesse, D. Atomic-scale study of electric dipoles near charged and uncharged domain walls in ferroelectric films. *Nat. Mater.* **2008**, *7*, 57−61.

(11) Kim, Y. M.; He, J.; Biegalski, M. D.; Ambaye, H.; Lauter, V.; Christen, H. M.; Pantelides, S. T.; Pennycook, S. J.; Kalinin, S. V.; Borisevich, A. Y. Probing oxygen vacancy concentration and homogeneity in solid-oxide fuel-cell cathode materials on the subunit-cell level. *Nat. Mater.* **2012**, *11*, 888−894.

(12) Yadav, A. K.; Nelson, C. T.; Hsu, S. L.; Hong, Z.; Clarkson, J. D.; Schlepuetz, C. M.; Damodaran, A. R.; Shafer, P.; Arenholz, E.; Dedon, L. R.; Chen, D.; Vishwanath, A.; Minor, A. M.; Chen, L. Q.; Scott, J. F.; Martin, L. W.; Ramesh, R. Observation of polar vortices in oxide superlattices. *Nature* **2016**, *530*, 198−201.

(13) Nellist, P. D. The principles of STEM Imaging. In *Scanning Transmission Electron Microscopy*; Pennycook, S. J., Nellist, P. D., Eds.; Springer: New York, 2011; pp 91−115.

(14) Krivanek, O. L.; Chisholm, M. F.; Nicolosi, V.; Pennycook, T. J.; Corbin, G. J.; Dellby, N.; Murfitt, M. F.; Own, C. S.; Szilagyi, Z. S.; Oxley, M. P.; Pantelides, S. T.; Pennycook, S. J. Atom-by-atom structural and chemical analysis by annular dark-field electron microscopy. *Nature* **2010**, *464*, 571−574.

(15) Kisielowski, C.; Wang, L.-W.; Specht, P.; Calderon, H. A.; Barton, B.; Jiang, B.; Kang, J. H.; Cieslinski, R. Real-time sub-Ångstrom imaging of reversible and irreversible conformations in rhodium catalysts and graphene. *Phys. Rev. B: Condens. Matter Mater. Phys.* **2013**, *88*, 024305.

(16) Van Dyck, D.; Jinschek, J. R.; Chen, F. R. 'Big Bang' tomography as a new route to atomic-resolution electron tomography. *Nature* **2012**, *486*, 243−246.

DOI: 10.1021/acs.nanolett.6b03331
Nano Lett. XXXX, XXX, XXX−XXX

(17) Chen, F. R.; Van Dyck, D.; Kisielowski, C. In-line three-dimensional holography of nanocrystalline objects at atomic resolution. *Nat. Commun.* **2016**, *7*, 10603.
(18) Huang, C.; Borisenko, K. B.; Kirkland, A. I. Exit wave reconstruction of radiation-sensitive materials from low-dose data. *J. Phys.: Conf. Ser.* **2014**, *522*, 012052.
(19) Meyer, R. R.; Sloan, J.; Dunin-Borkowski, R. E.; Kirkland, A. I.; Novotny, M. C.; Bailey, S. R.; Hutchison, J. L.; Green, M. L. H. Discrete atom imaging of one-dimensional crystals formed within single-walled carbon nanotubes. *Science* **2000**, *289*, 1324−1326.
(20) Wang, A.; Chen, F. R.; Van Aert, S.; Van Dyck, D. Direct structure inversion from exit waves. *Ultramicroscopy* **2010**, *110*, 527−534.
(21) Hsieh, W. K.; Chen, F. R.; Kai, J. J.; Kirkland, A. I. Resolution extension and exit wave reconstruction in complex HREM. *Ultramicroscopy* **2004**, *98*, 99−114.
(22) Yu, Y.; Zhang, X.; Zhao, Y. G.; Jiang, N.; Yu, R.; Wang, J. W.; Fan, C.; Sun, X. F.; Zhu, J. Atomic-scale study of topological vortex-like domain pattern in multiferroic hexagonal manganites. *Appl. Phys. Lett.* **2013**, *103*, 032901.
(23) Jinschek, J. R.; Yucelen, E.; Calderon, H. A.; Freitag, B. Quantitative atomic 3-D imaging of single/double sheet graphene structure. *Carbon* **2011**, *49*, 556−562.
(24) Kashtiban, R. J.; Dyson, M. A.; Nair, R. R.; Zan, R.; Wong, S. L.; Ramasse, Q.; Geim, A. K.; Bangert, U.; Sloan, J. Atomically resolved imaging of highly ordered alternating fluorinated graphene. *Nat. Commun.* **2014**, *5*, 4902.
(25) Linck, M.; Lichte, H.; Lehmann, M. Off-axis electron holography: Materials analysis at atomic resolution. *Int. J. Mater. Res.* **2006**, *97*, 890−898.
(26) Zheng, H.; Sadtler, B.; Habenicht, C.; Freitag, B.; Alivisatos, A. P.; Kisielowski, C. Controlling electron beam-induced structure modifications and cation exchange in cadmium sulfide-copper sulfide heterostructured nanorods. *Ultramicroscopy* **2013**, *134*, 207−213.
(27) McMullan, G.; Clark, A. T.; Turchetta, R.; Faruqi, A. R. Enhanced imaging in low dose electron microscopy using electron counting. *Ultramicroscopy* **2009**, *109*, 1411−1416.
(28) Buban, J. P.; Ramasse, Q.; Gipson, B.; Browning, N. D.; Stahlberg, H. High-resolution low-dose scanning transmission electron microscopy. *J. Electron Microsc.* **2010**, *59*, 103−112.
(29) Meyer, J. C.; Kotakoski, J.; Mangler, C. Atomic structure from large-area, low-dose exposures of materials: a new route to circumvent radiation damage. *Ultramicroscopy* **2014**, *145*, 13−21.

DOI: 10.1021/acs.nanolett.6b03331
Nano Lett. XXXX, XXX, XXX−XXX